2024 IEEE International Conference on Robotics and Automation (ICRA 2024)
May 13-17, 2024. Yokohama, Japan

Dynamic Interaction Control in Legged Mobile Manipulators: A Decoupled Approach

Qikai Li, Qinchen Meng, Yuxing Qin, Jiawei Chen, Xilun Ding, and Kun Xu*

***Abstract*— Legged mobile manipulators are receiving much more attention. Mobile platforms can infinitely expand the workspace of robotic arms, providing more possibilities for robot application scenarios. Compared with wheeled mobile manipulators, legged mobile manipulators have higher requirements for cooperative control of legged robots and robotic arms. This work decouples the control of the robotic arm and the legged robot. On the legged robot side, we explicitly estimate the wrench exerted by the robotic arm on the base and bring it into the legged robot's dynamics, and then use a nonlinear model predictive controller (NMPC) to control the legged robot. On the robotics arm side, we adopt an impedance controller to realize the end-effector's force control, and the introduction of impedance control has improved the safety and interactivity of legged mobile manipulators. We conducted experiments on physical robot to compare the differences between decoupled control and independent control, and the results show that the stability and robustness of robot systems have improved using decoupled control.**

I. INTRODUCTION

Mobile manipulation expands the task space of the robotic arm, has enriched the types of tasks that robots can achieve, and is one of the rising research highlights in the field of robotics. Traditional research on mobile manipulation is mainly on wheeled mobile robots and robotic arms, but this type of mobile manipulator is only suitable for flat ground. Recently, legged robots have shown improved terrain adaptability and maneuverability. The legged mobile manipulator will make up for the shortcomings of the wheeled mobile manipulator, which can perform tasks on flat or uneven surfaces. Thus, legged mobile manipulators have important application prospects in fields such as rescue, exploration, agriculture, inspection, and so on. Due to the robotic arm's minimal impact on the wheeled chassis, the control problem for wheeled mobile manipulation is fairly straightforward. However, for legged mobile manipulation, the robotic arm's movement has a significant impact on the stability of the legged robot. Therefore, a good design of legged robots and robotic arm controllers is crucial for the stable and reliable completion of tasks.

Impedance control has a wide range of applications in industrial robots, medical rehabilitation robots, service robots and other fields. Impedance control establishes a relationship between the motion of the end-effector and the external force, allowing for non-directive force control. Moreover, impedance control does not need additional contact sensors to determine when to switch between motion control and force control. Human-robot interaction can be made more natural and secure by modifying the impedance parameters of the robotic arm. Therefore, to ensure the robot's interactivity and safety, we also want the mobile manipulators to exhibit the impedance effect while performing tasks.

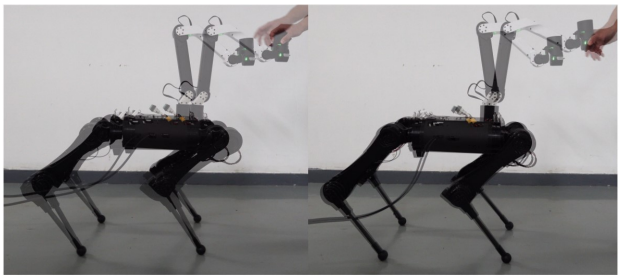

Fig. 1. The experimenter drags the arm when the quadruped is standing with independent control *(left)* and decoupled control *(right)*.

Two configurations of legged manipulator are common: quadruped robot with robotic arm and humanoid robot. For the quadruped robot with robotic arm, Boston Dynamics' [1] is a relatively early and remarkable work that used offline trajectory optimization to implement lifting and throwing heavy bricks on BigDog robot. They used body and leg movements to increase the weight lifted and distance thrown. [2] proposed a controller for quadruped manipulator using online motion planning and whole-body control (WBC). [3] presented a hydraulically driven quadruped manipulator and corresponding control methods. Because control systems for commercial quadruped robots are not often open-source, [4] developed a control method that treats the commercial quadruped as a black box in order to build a quadruped manipulator with commercial quadrupeds. [5] presented a framework for planning whole-body loco-manipulation trajectories robust to external disturbances. [6] proposed a mobile manipulation planning algorithm that can be solved in real time by neglecting the robot dynamics constraint. For the first time, [7] implement locomotion and manipulation using a unified model predictive control (MPC) framework, and operations such as end-effector position tracking and pulling heavy doors were implemented on the Anymal manipulator. [8] proposed a method that automatically discovers the whole-body motion trajectories jointly with contact schedules for solving general motion manipulation tasks in pre-modeled environments. The humanoid robot mobile operation research was carried out earlier and involved more,

The financial supports from the National Natural Science Foundation of China (52375003, U22B2080, T2121003) are grateful.

*Corresponding author

Authors are with the Robotics Institute, School of Mechanical Engineering and Automation, Beihang University, Beijing 100191, China; liqikai@buaa.edu.cn, qchmeng@buaa.edu.cn, starrr9@163.com, chenjiawei@buaa.edu.cn, xlding@buaa.edu.cn, xk007@buaa.edu.cn

including two-arm dexterous operation [9], maintaining body balance during operation [10], and whole-body motion planning control [11]. Boston Dynamics demonstrated the Altas humanoid robot's highly dynamic mobile manipulation capabilities [12], which is considered the primary goal of mobile manipulation for legged manipulator. Recently, there have also been some studies using reinforcement learning methods to control legged mobile manipulators [13]–[15].

The main contribution of this paper is to introduce the idea of impedance control into legged mobile manipulator, while decoupling the control of legged robots and robotic arms without affecting the original control strategy of the robotic arm. Compared with completely independent control, decoupled controller improves the robustness of the legged robot platform. The impedance control of the robotic arm ensures the interactivity, safety, and force control ability of the robot, which not only helps the application of legged mobile manipulators in human-robot cooperation, but also could perform complex force control operation tasks. We demonstrated the stability, dynamic interactivity, and force control ability of decoupled controller in the experiment.

II. FRAMEWORK

A. Overview

The framework of the whole control system is shown in Fig. (2). The whole controller is divided into two parts: the impedance controller of the robotic arm and the NMPC of the quadruped robot with WBC. In our method, the interaction wrench between the robotic arm and the quadruped body is considered. We estimate this wrench with the help of impedance control and use it as an input to the quadruped robot so that the MPC of the quadruped can take into account the influence of the robotic arm. This method is called decoupled control.

B. Impedance Control

The standard dynamic model of the robotic arm is:

$$\boldsymbol{\tau} = \boldsymbol{M}(\boldsymbol{\theta})\ddot{\boldsymbol{\theta}} + \boldsymbol{h}(\boldsymbol{\theta}, \dot{\boldsymbol{\theta}}), \tag{1}$$

where $\boldsymbol{\theta}$ is the vector of the arm joints' angles, $\boldsymbol{\tau}$ is the vector of joints' torques, $\boldsymbol{M}(\boldsymbol{\theta})$ is the symmetric positive-definite mass matrix, $\boldsymbol{h}(\boldsymbol{\theta}, \dot{\boldsymbol{\theta}})$ is the vector containing the Coriolis, the centripetal and the gravitational torques. When the dynamics is changed to task-space coordinates, it is formulated as:

$$\boldsymbol{\mathcal{F}} = \boldsymbol{\Lambda}(\boldsymbol{\theta})\dot{\boldsymbol{\mathcal{V}}} + \boldsymbol{\eta}(\boldsymbol{\theta}, \boldsymbol{\mathcal{V}}), \tag{2}$$

where

$$\begin{aligned} \boldsymbol{\Lambda}(\boldsymbol{\theta}) &= \boldsymbol{J}^{-T}\boldsymbol{M}(\boldsymbol{\theta})\boldsymbol{J}^{-1}, \\ \boldsymbol{\eta}(\boldsymbol{\theta}, \boldsymbol{\mathcal{V}}) &= \boldsymbol{J}^{-T}\boldsymbol{h}(\boldsymbol{\theta}, \boldsymbol{J}^{-1}\boldsymbol{\mathcal{V}}) - \boldsymbol{\Lambda}(\boldsymbol{\theta})\dot{\boldsymbol{J}}\boldsymbol{J}^{-1}\boldsymbol{\mathcal{V}}, \end{aligned} \tag{3}$$

and $\boldsymbol{\mathcal{F}}$ is external wrench applied to the end-effector, $\boldsymbol{\mathcal{V}}$ is the twist of the end-effector.

Impedance control models the end-effector as a spring-damped system in task-space. The impedance control law for the robotic arm is:

$$\boldsymbol{\tau}_{arm} = \boldsymbol{J}^{T}(\boldsymbol{\theta})\left(\widetilde{\boldsymbol{\Lambda}}(\boldsymbol{\theta})\ddot{\boldsymbol{x}} + \widetilde{\boldsymbol{\eta}}(\boldsymbol{\theta}, \dot{\boldsymbol{x}}) - \boldsymbol{\mathcal{F}}_{ext}\right), \tag{4}$$

$$\boldsymbol{\mathcal{F}}_{ext} = \boldsymbol{M}\ddot{\boldsymbol{x}} + \boldsymbol{B}\dot{\boldsymbol{x}} + \boldsymbol{K}\boldsymbol{x}, \tag{5}$$

where the task-space dynamics model $\{\tilde{\boldsymbol{\Lambda}}, \tilde{\boldsymbol{\eta}}\}$ is expressed in terms of the coordinates $\boldsymbol{x}$, $\boldsymbol{M}, \boldsymbol{B}, \boldsymbol{K}$ are coefficient matrices rendering mass, damping and stiffness, $\boldsymbol{\mathcal{F}}_{ext} = [\boldsymbol{f}_{ext}^T, \boldsymbol{\tau}_{ext}^T]^T$ is the external wrench acting on the arm's end-effector. Measurement of the acceleration $\ddot{\boldsymbol{x}}$ is likely to be noisy, so it is common to eliminate the mass compensation term $\widetilde{\boldsymbol{\Lambda}}(\boldsymbol{\theta})\ddot{\boldsymbol{x}}$ and to set $\boldsymbol{M} = 0$.

C. NMPC and WBC

Model Predictive Control, also known as Receding Horizon Control, solves an optimal control problem in receding way. The optimal control problem is formulated as:

$$\begin{aligned} \min_{\boldsymbol{x}(t), \boldsymbol{u}(t)} \quad & \underbrace{J\left(\boldsymbol{x}\left(t_F\right)\right)}_{\text{Mayer Term}} + \underbrace{\int_{t_0}^{t_F} L(\boldsymbol{x}(t), \boldsymbol{u}(t))dt}_{\text{Lagrange Term}} \\ \text{s.t.} \quad & \dot{\boldsymbol{x}}(t) = \boldsymbol{f}(\boldsymbol{x}(t), \boldsymbol{u}(t)) \\ & \boldsymbol{x}(0) = \boldsymbol{x}_0 \\ & + \text{other constraints}, \end{aligned} \tag{6}$$

where $\boldsymbol{x}(t) \in \mathbb{R}^{n_x}$ and $\boldsymbol{u}(t) \in \mathbb{R}^{n_u}$ are vectors of state and input variables. Lagrange term represents stage cost and Mayer term represents terminal cost. The problem is distinguished from a general numerical optimization problem by the fact that the independent variables are continuous functions with respect to time and the constraints contain first-order differential equation representing dynamic constraints. General methods for solving this problem are Differential Dynamic Programming (DDP) and Transcription methods.

1) System Dynamics

We use centroidal dynamics model to represent the quadruped's dynamics [16]. The centroidal dynamics model only takes into account the relationship between the whole system's momentum change rate and the external wrenches, ignoring the internal motion of the robot. In the legged mobile manipulator case, external wrenches contain feet forces and wrench between arm and body. The formulations of centroidal dynamics are:

$$\dot{\boldsymbol{h}}_{\text{com}} = \begin{bmatrix} \sum_{i=1}^{n_c} \boldsymbol{f}_{c_i} + \boldsymbol{f}_{inner} + m_q \boldsymbol{g} \\ \sum_{i=1}^{n_c} \boldsymbol{r}_{com,c_i} \times \boldsymbol{f}_{c_i} + \boldsymbol{\tau}_{inner} + \boldsymbol{\tau}_{c_i} \end{bmatrix}, \tag{7}$$

where m_q is quadruped robot's total mass, $\boldsymbol{r}$ is robot's center of mass and $\boldsymbol{h}_{com} = [\boldsymbol{p}_{com}^T, \boldsymbol{l}_{com}^T]^T$ represents the centroidal angular momentum. n_c is the number of contact points, $\boldsymbol{c}_i$ represents a contact point, $\{\boldsymbol{f}_{c_i}, \boldsymbol{\tau}_{c_i}\}$ are contact force and contact torque applied to the quadruped. $\boldsymbol{r}_{com,c_i}$ denotes the position of the contact point $\boldsymbol{c}_i$ with respect to the center of mass. $[\boldsymbol{f}_{inner}^T, \boldsymbol{\tau}_{inner}^T]^T$ is the inner wrench that the robotic arm applied to the quadruped base. The centroidal angular momentum $\boldsymbol{h}_{com}$ is linearly related to the generalized velocity $\boldsymbol{v}$, showing as:

$$\boldsymbol{h}_{com} = \underbrace{\begin{bmatrix} \boldsymbol{A}_b(\boldsymbol{q}) & \boldsymbol{A}_j(\boldsymbol{q}) \end{bmatrix}}_{\boldsymbol{A}(\boldsymbol{q})} \begin{bmatrix} \dot{\boldsymbol{q}}_b \\ \dot{\boldsymbol{q}}_j \end{bmatrix} \tag{8}$$

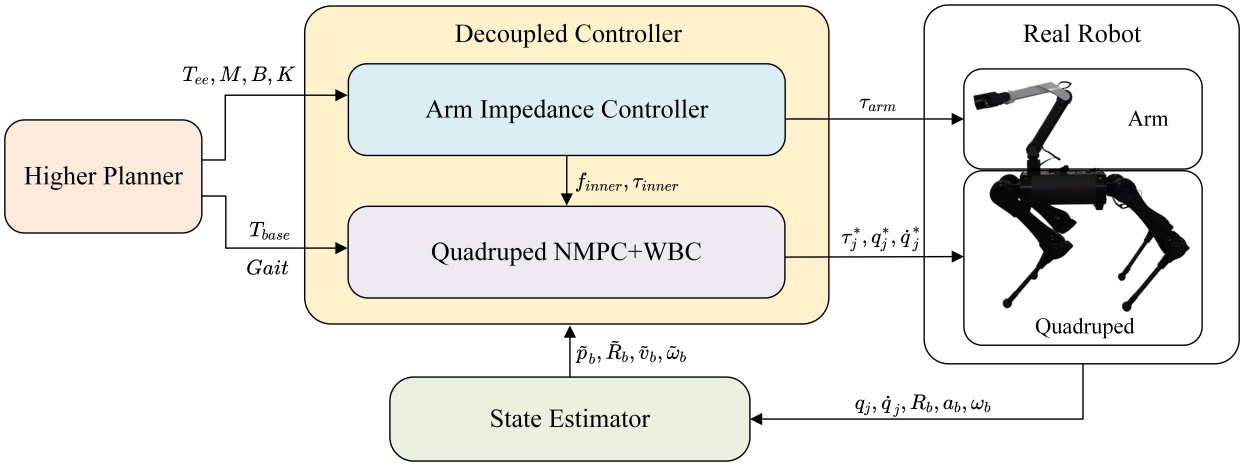

Fig. 2. A schematic diagram depicting the full control architecture. The end-effector's pose T_{ee}, coefficient matrices $\{M, B, K\}$, quadruped's base pose T_{base} and gait are provided by higher level planner.

where $\boldsymbol{A}(\boldsymbol{q})$ is called centroidal momentum matrix (CMM), $\boldsymbol{q}_b = [\boldsymbol{r}_b, \boldsymbol{\Phi}_b^{zyx}]^T \in \mathbb{R}^6$ is the base pose with respect to the inertial frame and $\boldsymbol{q}_j$ is the vector of quadruped joints coordinates.

Having laid down the foundations for defining physically consistent dynamics in our motion planner, we are now able to represent the quadruped as a dynamical system with state vector $\boldsymbol{x} = [\boldsymbol{h}_{com}, \boldsymbol{q}_b, \boldsymbol{q}_j]^T \in \mathbb{R}^{12+n_a}$ and input vector $\boldsymbol{u} = \left[\boldsymbol{f}_{c_1}, \ldots, \boldsymbol{f}_{c_{n_c}}, \boldsymbol{f}_{inner}, \boldsymbol{\tau}_{inner}, v_j\right]^T \in \mathbb{R}^{3\times n_c+6+n_a}$, where n_a represents the number of actuated joints.

2) Foot Constraints:

There are two types of robot foot constraints: support foot constraints and swing foot constraints. The foot should not slide relative to the ground when it is in contact with the ground, so the support force of the foot needs to be in the cone of friction and there is no relative motion of the foot with the ground, so the constraints for supporting the foot are:

$$f_{\min} \leq f_z \leq f_{\max} \tag{9a}$$
$$-\mu f_z \leq \pm f_x \leq \mu f_z \tag{9b}$$
$$-\mu f_z \leq \pm f_y \leq \mu f_z \tag{9c}$$

$$\boldsymbol{v}_{foot,sp} = 0, \tag{10}$$

where μ is the friction coefficient, $\boldsymbol{v}_{foot,sp}$ is supporting foot's velocity.

The swinging foot needs to track the desired swing trajectory, the reference trajectory of the swinging leg can be chosen from Bessel curves, pendulum lines, etc. The swinging foot is constrained to:

$$\boldsymbol{v}_{foot,sw} = \boldsymbol{v}_{ref} \tag{11}$$

where $\boldsymbol{v}_{foot,sp}$ is swing foot's velocity and $\boldsymbol{v}_{ref}$ is reference velocity.

3) Base Wrench Constraints:

Since the wrench of the robotic arm on the quadruped base is set as an input variable to the dynamics system of the quadruped robot, this inner wrench should be estimated to constrain the input variable. The wrench can be easily obtained if a six-dimensional wrench sensor was installed between the robotic arm base and quadruped body. Without using additional sensors, we propose a simplified method for estimating this wrench. The inner wrench can be divided into two parts: one part comes from the gravity and motion of the arm, and the other part is generated by the external force acting on the end-effector of the arm. For the first part, we assume the robotic arm moves slow and neglect the wrench produced by arm motion. Due to the use of impedance control for the robotic arm, the second part of the force can be estimated from the motion at the end. The inner wrench is estimated as:

$$\begin{aligned} \boldsymbol{f}_{arm} &= m_{arm}\boldsymbol{g} + \boldsymbol{f}_{ext} \\ \boldsymbol{\tau}_{arm} &= \boldsymbol{r}_{com,c_{arm}} \times m_{arm}\boldsymbol{g} \\ &\quad + \boldsymbol{r}_{com,c_{ee}} \times \boldsymbol{f}_{ext} + \boldsymbol{\tau}_{ext}, \end{aligned} \tag{12}$$

where m_{arm} is the total mass of robotic arm, $\boldsymbol{c}_{arm}$ denotes the point of robotic arm's center of mass and $\boldsymbol{c}_{ee}$ denotes the end-effector's contact point.

4) Whole-body Controller:

The optimal trajectories computed by the MPC are tracked through the WBC. Since the legged robot is a redundant system with high degrees of freedom, it can perform multiple motion tasks simultaneously. Compared to directly using inverse dynamics, WBC has better stability and robustness. A motion task $\boldsymbol{T}$ is expressed through a set of linear equality and/or inequality constraints on the solution vector $\boldsymbol{x} \in \mathbb{R}^{\ltimes}$, which is formulated as:

$$\mathrm{T}: \begin{cases} \boldsymbol{A}\boldsymbol{x} - \boldsymbol{b} = \boldsymbol{w} \\ \boldsymbol{D}\boldsymbol{x} - \boldsymbol{f} \leq \boldsymbol{v} \end{cases} \tag{13}$$

where $\boldsymbol{w}$ and $\boldsymbol{v}$ are slack variables to be minimized. A set of tasks $\boldsymbol{T}_1, \ldots, \boldsymbol{T}_p$ can be either solved at the same time, optionally weighted against each other, or in a strict prioritized order. We used a Hierarchical Quadratic Programming (HQP) approach to implement WBC, the tasks with low priority need to be implemented in the subspace of the high priority tasks' solutions. We search for a solution $\boldsymbol{x}$ in the space of

motion, torques and external force, resulting in

$$\boldsymbol{x} = [\ddot{\boldsymbol{q}}^T, \boldsymbol{\tau}_j^T, \boldsymbol{f}^T]^T \tag{14}$$

where $\boldsymbol{q} = [\boldsymbol{q}_b^T, \boldsymbol{q}_j^T]$ is the vector of quadruped's generalized coordinates, $\boldsymbol{\tau}_j$ is the vector of actuated joints' torques, $\boldsymbol{f} = [\boldsymbol{f}_{c_1}, \ldots, \boldsymbol{f}_{c_{n_c}}, \boldsymbol{f}_{inner}, \boldsymbol{\tau}_{inner}]$ is the vector of all the external forces.

The tasks that need to be done and the priority of the tasks are shown in the table I.

Dynamic consistency: The equations of motion of a mechanical system set a relationship between the generalized accelerations $\ddot{\boldsymbol{q}}$, the actuation torques $\boldsymbol{\tau}$ and external forces $\boldsymbol{f}$ as:

$$\boldsymbol{M}\ddot{\boldsymbol{q}} - \boldsymbol{\tau}_j - \boldsymbol{J}^T\boldsymbol{f} = \boldsymbol{h}(\dot{\boldsymbol{q}}, \boldsymbol{q}) \tag{15}$$

where $\boldsymbol{J}$ is the stack of Jacobian matrices for all external force action points.

Contact motion constraints: Since legs in contact with the ground are not allowed to move, $\boldsymbol{J}\dot{\boldsymbol{q}} = \boldsymbol{0}$ is required to ensure contact consistency. To write the task in standard form, differentiate the two sides of the equation:

$$\boldsymbol{J}\ddot{\boldsymbol{q}} = -\dot{\boldsymbol{J}}\boldsymbol{q} \tag{16}$$

Friction cone constraints: These constraints are the same as those in MPC, as shown in Eq.(9)

Torque limits: To ensure that the solution complies with the hardware limitations defined by minimum $\boldsymbol{\tau}_{min}$ and maximum $\boldsymbol{\tau}_{max}$ admissible torques, the joint torques should be:

$$\boldsymbol{\tau}_{min} \leq \boldsymbol{\tau}_j \leq \boldsymbol{\tau}_{max} \tag{17}$$

Base motion tracking: We use a PD controller to realize base motion tracking, formulated as:

$$\ddot{\boldsymbol{q}}_b = \boldsymbol{K}_p(\boldsymbol{\mathcal{S}}_{ref} - \boldsymbol{\mathcal{S}}_{meas}) + \boldsymbol{K}_d(\boldsymbol{\mathcal{V}}_{ref} - \boldsymbol{\mathcal{V}}_{meas}) \tag{18}$$

where $\mathcal{S}$ is the screw representation of quadruped base's transformation, $\mathcal{V}$ is the velocity twist. $\boldsymbol{K}_d$ and $\boldsymbol{K}_d$ are proportional and differential matrices. The reference value comes from MPC's solution.

Swing legs motion tracking: Similar to base motion tracking, swing legs also use PD controller to track. For a swing leg, the formulation is:

$$\boldsymbol{J}_i\ddot{\boldsymbol{q}} = -\dot{\boldsymbol{J}}_i\boldsymbol{q} + \boldsymbol{a}_{ref} + \boldsymbol{K}_p(\boldsymbol{p}_{ref} - \boldsymbol{p}_{meas}) + \boldsymbol{K}_d(\boldsymbol{v}_{ref} - \boldsymbol{v}_{meas}) \tag{19}$$

where $\boldsymbol{J}_i$ is the Jacobian of swing leg's foot, $\boldsymbol{p}$ and $\boldsymbol{v}$ are the foot's position and velocity. Also, the reference value comes from MPC's solution.

Contact forces: The support force applied to the feet of the quadruped robot and the wrench exerted by the robotic arm on the robot base should be the same as the calculation result of MPC:

$$\boldsymbol{f} = \boldsymbol{f}_{ref} \tag{20}$$

All the tasks can be reformulated to the standard form of linear equality and/or inequality constriants. For a detailed discussion on how the QP structure is set up and solved, the reader is referred to the relevant papers [17], [18].

TABLE I
WBC TASKS AND PRIORITIES

Priority	Task
1	Dynamic consistency Contact motion constraints
2	Friction cone constraints Torque limits
3	Base motion tracking Swing leg motion tracking Contact force

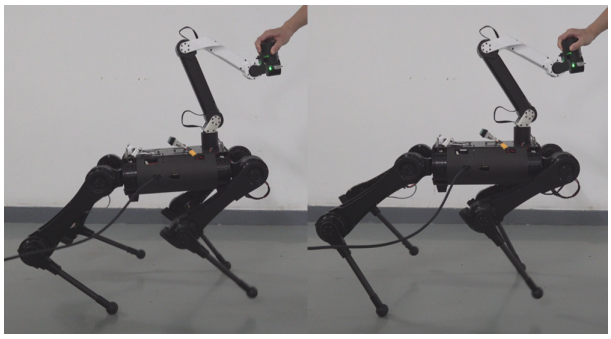

Fig. 3. The experimenter drags the arm when the quadruped is trotting with independent control *(left)* and decoupled control *(right)*.

III. SYSTEM DESCRIPTION

The framework described in the previous section is applicable to a variety of multi-branch legged manipulator robotic systems. In this work, we validate the feasibility of our approach on a quadruped mobile manipulator. This quadruped mobile manipulator consists of a 12-degree-of-freedom quadruped robot and a 6-degree-of-freedom robotic arm. All joints of the robot use semi-direct-drive motors, thus allowing joint level torque control. The overall weight of the quadruped robot is 19kg and the weight of the robotic arm is 3kg.

All controllers run on an on-board computer (Intel Core i7 8850H CPU@4GHz hexacore processor) that the robot is equipped with. With a time horizon of $T = 1s$, the MPC is computed at a frequency of 50Hz. The WBC is computed at a frequency of 500Hz. Both the MPC and the WBC obtain the estimated base frame information from the state estimator, including the base speed and position. The state estimator uses the methodology in paper [19]. We use OCS2 software framework [20] to solve the MPC problem.

IV. EXPERIMENTS

We conducted three types of experiments on the physical robot, namely: 1. decoupled control versus independent control. 2. decoupled control versus whole-body MPC. 3. end force control experiment using decoupled control. Independent control means that the control of the quadruped robot and the robotic arm are completely separated, without considering the interaction between the robotic arm and the quadruped robot. For more details, see supplementary videos[1].

[1]https://youtu.be/595Of5cipf0

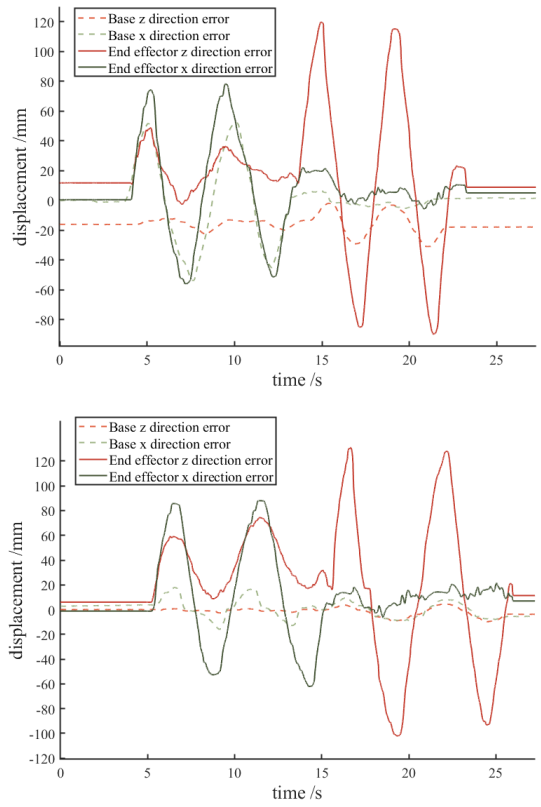

Fig. 4. Robotic arm's end-effector and quadruped base's movement with respect to time with decoupled control *(up)* and independent control *(down)*.

A. Experiments comparing decoupled control and independent control

In this experiment, our main objective is to verify that the decoupled method can enhance the stability of the quadruped robot compared with independent method. The experiment is accomplished under the standing state and trotting state of the quadruped robot. Because the measured end-effector acceleration $\ddot{\boldsymbol{x}}$ is noisy, the mass matrix $\boldsymbol{M}$ in impedance control was set 0. The coordinates $\boldsymbol{x}$ were chose as end-effector's position and Euler angle, so that $\boldsymbol{x} = [\boldsymbol{r}_{ee}, \boldsymbol{\Phi}_{ee}^{zyx}]^T$. Due to the experimental phenomenon being more pronounced in the translational direction, the diagonal elements of stiffness matrix and damping matrix was set as $diag(\boldsymbol{K}) = [250, 250, 250, 2500, 2500, 2500]^T$ and $diag(\boldsymbol{B}) = [10, 10, 10, 50, 50, 50]^T$. The impedance parameters of the robotic arm are exactly the same in all the experiments.

When the quadruped manipulator was in standing state with height of $0.5m$, the experimenter drags the robot arm's end-effector. As is shown in Fig. 1, in the independent control experiment, the quadruped robot moves considerably with the dragging of the robot arm; while in the decoupled control, the body of the quadruped robot hardly moves with the dragging of the robot arm. Fig. 4 plots the quadruped body and arm's end-effector displacement in the x and z direction over time for the two control methods. Also, it can be seen that the quadruped base moves much less using decoupled control, which means the quadruped base will be more stable when robotic arm is operating with large force. In addition, independent control cannot compensate for the gravity of the robotic arm, so there is a static error in the height of the quadruped robot body from the expected height. Due to friction in the robotic arm joints, there is also static error at the end of the robotic arm.

When dragging the robot arm, situation in trotting state is similar to that in the standing state. Fig. 3 shows that under decoupled control, when the experimenter pushes the end of the robotic arm, the quadruped robot adjusts the position of the landing point to resist external forces; while under independent control, the quadruped robot will not make corresponding adjustments. This indicates that in a dynamic gait state, even if the robotic arm has a large operating force, decoupled control can ensure the stability of the quadruped robot.

TABLE II

COMPUTATION TIME OF DECOUPLED QUADRUPED MPC AND WHOLE-BODY MPC

Procedure	Decoupled quadruped MPC (ms)	Whole-body MPC (ms)
LQ approximation	2.89882	4.78872
Solve QP	0.800249	1.82555
Linesearch	0.252201	0.454792
Compute controller	0.0155825	0.0213223

B. Experiments comparing decoupled control and whole-body MPC

We compared the decoupled control with the whole-body MPC proposed in [7] in the simulation. Both methods in simulation can achieve stable control of robots. However, compared to the decoupled quadeuped MPC, the whole-body MPC has a higher dimension of variables, resulting in a longer solution time. We used the built-in timer in OCS2 to count the calculation time of MPC, as shown in the table II. The computer CPU used for simulation is 11th Intel i5-11400F, and both controllers use sequential quadratic programming (SQP) with 4 threads for computation. Due to the negligible computation time of the impedance controller compared to MPC, our proposed decoupled controller has an advantage in total computation time and is more suitable for embedded computers in robots.

Unfortunately, we were unable to successfully deploy the whole-body MPC onto the physical robot. Using whole-body MPC, when the robot switches from stance to trot gait, it will shake violently and lose stability. We speculate that the reason is that the introduction of the robotic arm in the dynamic model reduces the robustness of the whole-body MPC. Thus, the unmodeled joint friction, dynamic parameter errors, and vibration of the robotic arm result in the divergence of whole-body MPC. In order to deploy whole-body MPC on real machines, there are still many engineering problems to be solved.

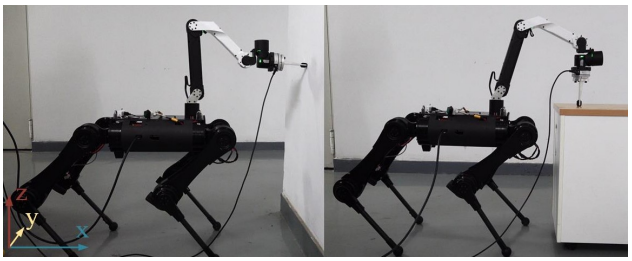

Fig. 5. Quadruped mobile manipulator pushes with commanded force in x (*left*) and z (*right*) direction while standing.

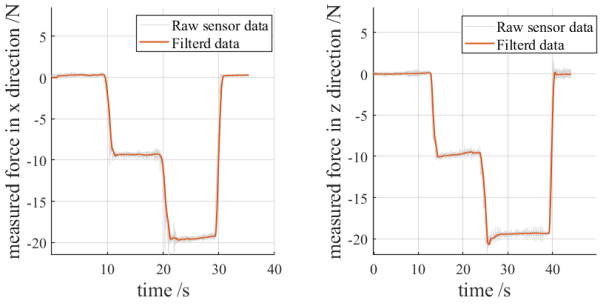

Fig. 6. Plots showing measured raw force data and filtered force data in x (*left*) and z (*right*) direction while quadruped is standing.

C. Force control experiment

The purpose of this experiment is to verify that a quadruped mobile manipulator robot can utilize the impedance property of the robotic arm to achieve end-force control. Similar to the previous experiment, the experiment consists of two parts: the quadruped robot in the standing state and the quadruped robot in the dynamic trotting state. Measurement of the end manipulation force of the robotic arm was obtained by a six-dimensional force sensor mounted at the end. In the standing state, the robot applied forces in x and z direction as shown in Fig. 5. The commanded force was 10N and 20N in both configuration. As is shown in Fig. 6, measured force tracks the expected force well. Due to the lack of modeling of joint friction, there is a static error between the output force of the robotic arm and the expected force. In the trotting state, the robot applied forces in x direction and the commanded force was 10N. Fig. 7 shows the raw force data and filtered force data. Due to the body shaking caused by trot gait, there is significant noise in the original measurement data. The filtered data indicates that the average force applied by the robotic arm is relatively close to the expected force.

V. CONCLUSIONS

In this work, we propose a decoupling control method that combines impedance control of a robotic arm with NMPC control of a quadruped robot. In the process of establishing the dynamics of a quadruped robot, we considered the force between the robotic arm and the body, and estimated the force exerted by the robotic arm on the body using the impedance model of the robotic arm. Compared with the completely independent control of the robotic arm and

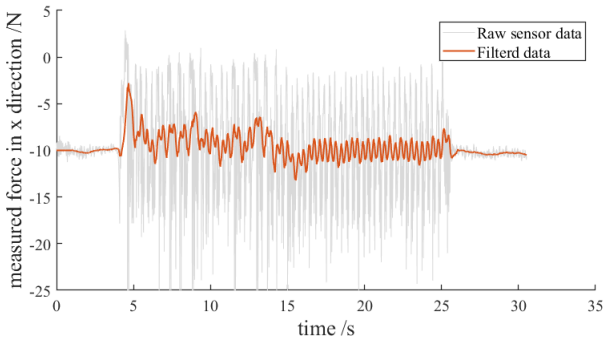

Fig. 7. Plots showing measured raw force data and filtered force data in x direction while quadruped is trotting.

quadruped, decoupled control considers the influence of the robotic arm on the quadruped robot during operation. We carried out experiments on actual robots and showed that, in the presence of interference from external forces, the robustness of quadruped robots is enhanced in both the standing and dynamic walking states. Due to the use of impedance control in the robotic arm, the robot does not need to switch between force control and position control through additional means to obtain the contact state between the robotic arm and the environment. One of the natural extensions to this work would be variable impedance control of safety and energy perception, which is of great significance for scenarios that require human-robot cooperation.

REFERENCES

[1] M. P. Murphy, B. Stephens, Y. Abe, and A. A. Rizzi, "High degree-of-freedom dynamic manipulation," in *Unmanned Systems Technology XIV*, vol. 8387. International Society for Optics and Photonics, May 2012, p. 83870V. [Online]. Available: https://www.spiedigitallibrary.org/conference-proceedings-of-spie/8387/83870V/High-degree-of-freedom-dynamic-manipulation/10.1117/12.919939.short

[2] C. D. Bellicoso, K. Krämer, M. Stäuble, D. Sako, F. Jenelten, M. Bjelonic, and M. Hutter, "ALMA - Articulated Locomotion and Manipulation for a Torque-Controllable Robot," in *2019 International Conference on Robotics and Automation (ICRA)*, May 2019, pp. 8477–8483, iSSN: 2577-087X.

[3] B. U. Rehman, M. Focchi, J. Lee, H. Dallali, D. G. Caldwell, and C. Semini, "Towards a multi-legged mobile manipulator," in *2016 IEEE International Conference on Robotics and Automation (ICRA)*. Stockholm, Sweden: IEEE, May 2016, pp. 3618–3624. [Online]. Available: http://ieeexplore.ieee.org/document/7487545/

[4] S. Zimmermann, R. Poranne, and S. Coros, "Go Fetch! - Dynamic Grasps using Boston Dynamics Spot with External Robotic Arm," in *2021 IEEE International Conference on Robotics and Automation (ICRA)*. Xi'an, China: IEEE, May 2021, pp. 4488–4494. [Online]. Available: https://ieeexplore.ieee.org/document/9561835/

[5] H. Ferrolho, V. Ivan, W. Merkt, I. Havoutis, and S. Vijayakumar, "RoLoMa: Robust Loco-Manipulation for Quadruped Robots with Arms," *arXiv:2203.01446 [cs]*, Mar. 2022, arXiv: 2203.01446. [Online]. Available: http://arxiv.org/abs/2203.01446

[6] P. Ewen, J.-P. Sleiman, Y. Chen, W.-C. Lu, M. Hutter, and R. Vasudevan, "Generating Continuous Motion and Force Plans in Real-Time for Legged Mobile Manipulation," in *2021 IEEE International Conference on Robotics and Automation (ICRA)*, May 2021, pp. 4933–4939, iSSN: 2577-087X.

[7] J.-P. Sleiman, F. Farshidian, M. V. Minniti, and M. Hutter, "A Unified MPC Framework for Whole-Body Dynamic Locomotion and Manipulation," *IEEE Robotics and Automation Letters*, vol. 6, no. 3, pp. 4688–4695, Jul. 2021, conference Name: IEEE Robotics and Automation Letters.

[8] J.-P. Sleiman, F. Farshidian, and M. Hutter, "Versatile multicontact planning and control for legged loco-manipulation," *Science Robotics*, vol. 8, no. 81, p. eadg5014, Aug. 2023, publisher: American Association for the Advancement of Science. [Online]. Available: https://www.science.org/doi/10.1126/scirobotics.adg5014

[9] C. Ott, O. Eiberger, W. Friedl, B. Bauml, U. Hillenbrand, C. Borst, A. Albu-Schaffer, B. Brunner, H. Hirschmuller, S. Kielhofer, R. Konietschke, M. Suppa, T. Wimbock, F. Zacharias, and G. Hirzinger, "A Humanoid Two-Arm System for Dexterous Manipulation," in *2006 6th IEEE-RAS International Conference on Humanoid Robots*, Dec. 2006, pp. 276–283, iSSN: 2164-0580.

[10] K. Harada, S. Kajita, K. Kaneko, and H. Hirukawa, "Dynamics and balance of a humanoid robot during manipulation tasks," *IEEE Transactions on Robotics*, vol. 22, no. 3, pp. 568–575, Jun. 2006, conference Name: IEEE Transactions on Robotics.

[11] L. Sentis, J. Park, and O. Khatib, "Compliant Control of Multicontact and Center-of-Mass Behaviors in Humanoid Robots," *IEEE Transactions on Robotics*, vol. 26, no. 3, pp. 483–501, Jun. 2010, conference Name: IEEE Transactions on Robotics.

[12] Boston Dynamics, "Atlas Gets a Grip | Boston Dynamics," Jan. 2023. [Online]. Available: https://www.youtube.com/watch?v=-e1_QhJ1EhQ

[13] Y. Ma, F. Farshidian, T. Miki, J. Lee, and M. Hutter, "Combining Learning-Based Locomotion Policy With Model-Based Manipulation for Legged Mobile Manipulators," *IEEE Robotics and Automation Letters*, vol. 7, no. 2, pp. 2377–2384, Apr. 2022, conference Name: IEEE Robotics and Automation Letters.

[14] Y. Ma, F. Farshidian, and M. Hutter, "Learning Arm-Assisted Fall Damage Reduction and Recovery for Legged Mobile Manipulators," Mar. 2023, arXiv:2303.05486 [cs]. [Online]. Available: http://arxiv.org/abs/2303.05486

[15] Z. Fu, X. Cheng, and D. Pathak, "Deep Whole-Body Control: Learning a Unified Policy for Manipulation and Locomotion," Aug. 2022. [Online]. Available: https://openreview.net/forum?id=zldI4UpuG7v

[16] D. E. Orin, A. Goswami, and S.-H. Lee, "Centroidal dynamics of a humanoid robot," *Autonomous Robots*, vol. 35, no. 2, pp. 161–176, Oct. 2013. [Online]. Available: https://doi.org/10.1007/s10514-013-9341-4

[17] C. Dario Bellicoso, C. Gehring, J. Hwangbo, P. Fankhauser, and M. Hutter, "Perception-less terrain adaptation through whole body control and hierarchical optimization," in *2016 IEEE-RAS 16th International Conference on Humanoid Robots (Humanoids)*, Nov. 2016, pp. 558–564, iSSN: 2164-0580.

[18] C. Dario Bellicoso, F. Jenelten, P. Fankhauser, C. Gehring, J. Hwangbo, and M. Hutter, "Dynamic locomotion and whole-body control for quadrupedal robots," in *2017 IEEE/RSJ International Conference on Intelligent Robots and Systems (IROS)*, Sep. 2017, pp. 3359–3365, iSSN: 2153-0866.

[19] J. Di Carlo, P. M. Wensing, B. Katz, G. Bledt, and S. Kim, "Dynamic Locomotion in the MIT Cheetah 3 Through Convex Model-Predictive Control," in *2018 IEEE/RSJ International Conference on Intelligent Robots and Systems (IROS)*. Madrid: IEEE, Oct. 2018, pp. 1–9. [Online]. Available: https://ieeexplore.ieee.org/document/8594448/

[20] F. Farshidian *et al.*, "OCS2: An open source library for optimal control of switched systems," [Online]. Available: https://github.com/leggedrobotics/ocs2.